CPL calculations of [7]helicenes with alleged exceptional emission dissymmetry values

Ciro A. Guido, Francesco Zinna and Gennaro Pescitelli

Supporting Information

Contents

Table S1. Key structural parameters measured on the X-ray structures of **1** and **3** and on (TD)-DFT optimized ground-state (GS) and excited-state (ES) structures of **1a**, **2a** and **3** at PBE0-1/3-D3BJ/6-311+G(d,p) level.

Table S2. Key structural parameters measured on (TD)-DFT optimized ground-state (GS) and excited-state (ES) structures of **1a**, **2a** and **3** at (CAM-)B3LYP-D3BJ/6-311+G(d,p) level.

Table S3. Key parameters for the S_0-S_1 transition calculated on (*M*)-**1a** with CAM-B3LYP/*basis_set*//CAM-B3LYP/6-31+G(d) level in gas phase with various basis sets.

Table S4. Key parameters for the S_1-S_0 transition calculated on (*M*)-**1a** with CAM-B3LYP/*basis_set*//CAM-B3LYP/6-31+G(d) level in gas phase with various basis sets.

Table S5. Impact of solvent model on chiroptical computed data of [7]helicene *M*-**3**.

Table S6. Key structural parameters measured on (TD)-DFT optimized ground-state (GS) and excited-state (ES) structures of phenanthrene staked dimers **Phen$_2$**. Selected structures and relative energies are reported in Figure S3.

Table S7. Key chiroptical computed data for the dimer (*M,M*)-**2a$_2$**. Structures are reported in Figure S4.

Table S8. Key experimental and calculated chiroptical data extracted from a literature survey on helicenes. Graphical correlation shown below.

Figure S1. Comparison of GS (dark orange) and ES (green) geometries of *M*-**1a**, *M*-**2a** and *M*-**3** calculated at PBE0-1/3-D3BJ/6-311+G(d,p) level in the gas phase, seen along the C_2 axis.

Figure S2. Comparison of GS (dark orange) and ES (green) geometries of *M*-**1a**, *M*-**2a** and *M*-**3** calculated at (CAM)-B3LYP-D3BJ/6-311+G(d,p) level in the gas phase, seen along the C_2 axis.

Figure S3. Selected geometries and energies for (TD)-DFT optimized ground-state (GS) and excited-state (ES) structures of phenanthrene stacked dimers **Phen$_2$**. All calculations run with D3BJ dispersion correction and 6-311+G(d,p) basis set. Top and side views are shown for each geometry.

Figure S4. Geometries of (TD)-DFT optimized ground-state (GS) and excited-state (ES) structures of dimers (*M,M*)-**2a$_2$**.

Figure S5. Schematic illustration the steps necessary to compute emissive properties in a state specific approach.

State-specific (SS) description of emission dissymmetry factors

References for the Supporting Information

Table S1. Key structural parameters measured on the X-ray structures of **1** and **3** and on (TD)-DFT optimized ground-state (GS) and excited-state (ES) structures of **1a**, **2a** and **3** at PBE0-1/3-D3BJ/6-311+G(d,p) level.

	Helical twist (A)[a,b] / deg	Diene torsion (B)[a,c] / deg	Terminal inter-ring distance (C)[a,d] / Å
1 (*exp*)[e]	*97.8*	*17.9*	*4.04*
1a GS (calc)[f]	99.1	13.3	3.80
1a ES (calc)[f]	100.0	15.6	3.76
2a GS (calc)[f]	96.6	11.7	3.76
2a ES (calc)[f]	100.2	14.9	3.75
3 (*exp*)[g]	*86.9*	*12.7*	*4.04*
3 GS (calc)[f]	86.3	13.2	3.73
3 ES (calc)[f]	93.6	10.5	3.77

[a] See figure below for definition (shown on **3**); absolute values reported. [b] Sum of 5 dihedral angles from C1 to C8. [c] Of the formal diene moiety of the 5-membered ring. [d] Between the centroids. [e] X-ray structure from ref. 1. [f] PBE0-1/3-D3BJ/6-311+G(d,p) calculations in gas phase. [g] X-ray structure from ref. 2.
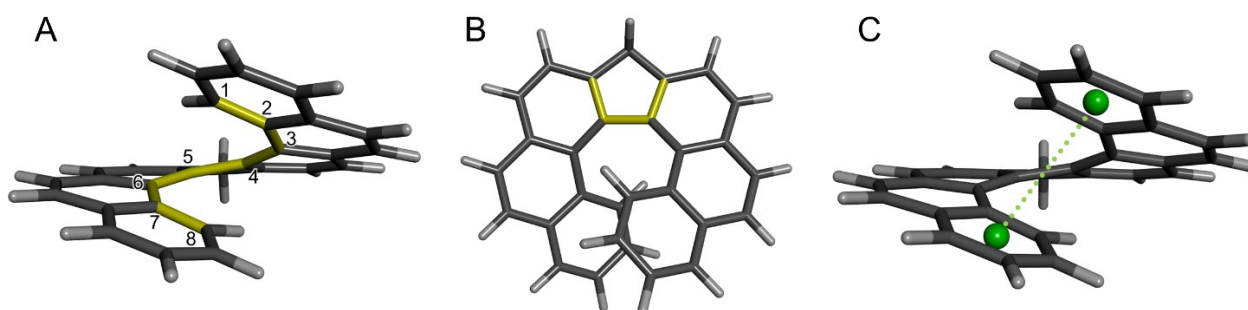

Table S2. Key structural parameters measured on (TD)-DFT optimized ground-state (GS) and excited-state (ES) structures of **1a**, **2a** and **3** at (CAM-)B3LYP-D3BJ/6-311+G(d,p) level.

	Helical twist (A)[a,b] / deg	Diene torsion (B)[a,c] / deg	Terminal inter-ring distance (C)[a,d] / Å
1a GS (calc)[e]	99.4	13.3	3.77
1a ES (calc)[f]	101.1	15.8	3.84
2a GS (calc)[e]	96.9	11.7	3.75
2a ES (calc)[f]	101.0	15.2	3.83
3 GS (calc)[e]	86.6	13.2	3.73
3 ES (calc)[f]	94.1	17.4	3.87

[a] See figure below Table S1 for definition (shown on **3**); absolute values reported. [b] Sum of 5 dihedral angles from C1 to C8. [c] Of the formal diene moiety of the 5-membered ring. [d] Between the centroids. [e] B3LYP-D3BJ/6-311+G(d,p) calculations in gas phase. [g] CAM-B3LYP-D3BJ/6-311+G(d,p) calculations in gas phase starting from GS structures.

Table S3. Key parameters for the S_0-S_1 transition calculated on (*M*)-**1a** with CAM-B3LYP/*basis_set*//CAM-B3LYP/6-31+G(d) level in gas phase with various basis sets.

basis_set	No. of bases	Energy / eV	*R* (velocity gauge) / 10^{-40} cgs	*R* (length gauge) / 10^{-40} cgs	%diff.
6–31+G(d)	1033	3.60	−142.7	−142.3	0.3
6–311+G(d,p)	1314	3.58	−146.1	−146.2	0.1
cc–pVTZ	1978	3.58	−155.2	−151.4	2.5
aug–cc–pVTZ	3082	3.56	−147.4	−147.5	0.1

[a] Percent difference between rotational strength calculated with velocity and length gauge. The negligible difference obtained with 6-311+G(d,p) is an indication of basis set completeness.

Table S4. Key parameters for the S_1-S_0 transition calculated on (*M*)-**1a** with CAM-B3LYP/*basis_set*//CAM-B3LYP/6-31+G(d) level in gas phase with various basis sets.

basis_set	No. of bases	Energy / eV	*R* (velocity gauge) / 10^{-40} cgs	*R* (length gauge) / 10^{-40} cgs	%diff.
6-31+G(d)	1033	2.67	−225.3	−228.0	1.2
6-311+G(d,p)	1314	2.64	−228.7	−230.6	0.8
cc-pVTZ	1978	2.64	−242.7	−237.3	2.2
aug-cc-pVTZ	3082	2.63	−229.1	−229.9	0.4

[a] Percent difference between rotational strength calculated with velocity and length gauge. The negligible difference obtained with 6-311+G(d,p) is an indication of basis set completeness.

Table S5. Impact of solvent model on chiroptical computed data of [7]helicene *M*-**3**.

Method[a]	Model[b]	λ_{max}[c]	g_{abs}[d]	λ_{em}[c]	g_{lum}[d]	Stokes shift[e]	g_{lum}/g_{abs}
a	Gas	348	−1.0	434	−4.9	0.71	4.9
a	LR-PCM	355	−0.78	444	−3.1	0.70	3.9
a	VEM-UD	352	−1.4	434	−5.1	0.67	3.6
b	Gas	361	−1.1	447	−5.3	0.66	4.8
b	LR-PCM	367	−0.87	453	−3.4	0.64	3.9
b	VEM-UD	363	−1.5	444	−5.8	0.62	3.8

[a] Method (*a*): CAM-B3LYP-D3BJ/6-311+G(d,p)//B3LYP-D3BJ/6-311+G(d,p); method (*b*): PBE0-1/3-D3BJ/ 6-311+G(d,p)//PBE0-1/3-D3BJ/6-311+G(d,p). [b] Solvent model: gas phase (gas); linear-response PCM (LR-PCM) for $CHCl_3$; vertical excitation method with unrelaxed ES density (VEM-UD) for $CHCl_3$. [c] In nm. [d] Multiplied by 10^{-3}. [e] In eV.

Table S6. Key structural parameters measured on (TD)-DFT optimized ground-state (GS) and excited-state (ES) structures of phenanthrene stacked dimers **Phen$_2$**. Selected structures and relative energies are reported in Figure S3.

Structure		Method[a]	Horizontal offset (HO)[b] / Å	Vertical offset (VO)[b] / Å	Plane-to-plane distance (d)[b] / Å	Twist angle (τ)[b] / °
Experimental[c]		–	*0.0*	*1.66(3)*	*3.44(2)*	*0.0*
Phen$_2$-A	GS (calc)	B3LYP	1.65	0.0	3.36	0.0
	GS (calc)	CAM-B3LYP	1.64	0.0	3.46	0.0
	ES (calc)	CAM-B3LYP	2.43	0.0	3.00	0.0
	GS (calc)	PBE-1/3	1.64	0.0	3.39	0.0
	ES (calc)	PBE-1/3	2.18	0.0	2.96	0.0
Phen$_2$-B	GS (calc)	B3LYP	0.43	1.52	3.34	0.0
	GS (calc)	CAM-B3LYP	0.43	1.51	3.44	0.0
	ES (calc)	CAM-B3LYP	0.35	0.04	2.92	14.2
	GS (calc)	PBE-1/3	0.44	1.52	3.37	0.0
	ES (calc)	PBE-1/3	0.41	0.05	2.91	14.1

[a] The D3BJ dispersion correction and 6-311+G(d,p) basis set were employed in all cases. Calculations run in gas phase.
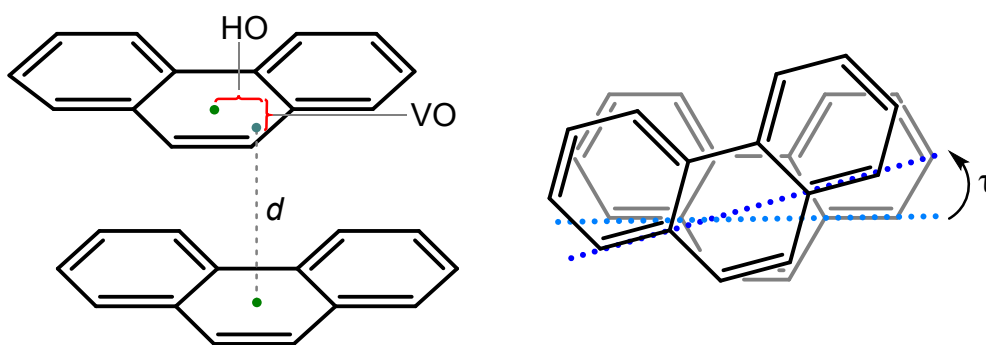[b] See figure below for definition. [c] X-ray structure from ref. 3.

Table S7. Key chiroptical computed data for the dimer (*M*,*M*)-**2a$_2$**. Structures are reported in Figure S4.

Model	λ_{max}[a,c]	g_{abs}[b,c]	λ_{em}[a,d]	g_{lum}[b,d]	Stokes shift[e]	g_{lum}/g_{abs}
Gas	344	−5.2	461	−7.3	0.91	1.4
LR-PCM	345	−3.4	465	−4.3	0.93	1.2

[a] In nm. [b] Multiplied by 10^{-3}. [c] Calculated at CAM-B3LYP/6-31G+(d)//B3LYP-D3BJ/6-31G+(d) level. [e] Calculated at CAM-B3LYP/6-31G+(d)//CAM-B3LYP-D3BJ/6-31G+(d) level. [e] In eV.

Table S8. Key experimental and calculated chiroptical data extracted from a literature survey on helicenes.[a] Graphical correlation shown below.

Type	λ_{max}[b] (exp)	g_{abs}[c] (exp)	λ_{em}[b] (exp)	g_{lum}[c] (exp)	Stokes Shift[b] (exp)	g_{lum}/g_{abs} (exp)	g_{abs}[c] (calc)	g_{lum}[c] (calc)	Stokes Shift[b] (calc)	g_{lum}/g_{abs} (calc)	Reference	Molecule[d]
hetero [6]helicene	411	4.7	427	4.2	16	0.90	4.5	7.0	37	1.6	4	1
carbo [6]helicene	412	0.9	421	1.1	9	1.2	2.7	7.1	34	2.6	4	2
carbo [6]helicene	420	0.6	422	0.08	2	0.14	0.55	4.25	34	7.7	4	3
carbo [6]helicene	427	4.5	527	1.8	100	0.4	2.7	1.8	42	0.67	5	1e
carbo [6]helicene	427	6.0	520	3.1	93	0.5	2.7	3.1	34	1.1	5	2e
carbo [6]helicene	391	30	450	6	59	0.2	50	−8[f]	61	−0.16	6	1
carbo [6]helicene	418	16	500	3	82	0.2	24	5	80	0.21	6	2
carbo [6]helicene	421	16	550	13	129	0.8	18	18	122	1	6	3
hetero [6]helicene	395	18	483	9	88	0.5	11	13	102	1.2	7	2
hetero [9]helicene	460	12	548	27	88	2.2	66	52	105	0.79	8	9Ha
carbo [7]helicene	569	2.3	652	2.7	83	1.2	2.7	4.0	193	1.5	9	1
carbo [5]helicene	381	1.5	453	1.9	72	1.3	1.4	1.3	100	1.1	10	2d
carbo [6]helicene	327	10	421	1	94	9.4	8.5	1.3	57	0.15	11	H6
carbo [6]helicene	341	20	422	9	81	4.0	19	21	48	1.1	11	H6(H)2
carbo [6]helicene	382	32	426	28	44	0.87	18	71	18	3.9	11	H6(CN)2
carbo [6]helicene	428	22	500	54	72	2.4	20	34	106	1.7	11	H6(NMe2)2
hetero [7]helicene	425	–	430	1.1	5	–	–	0.66	49	–	12	C-29
hetero [7]helicene	475	–	585	1.2	110	–	–	0.78	103	–	12	C-29H+
carbo [4]helicene	413	0.28	424	1.2	11	4.3	3.5 [g]	2	59	0.57	13	2°
carbo [4]helicene	392	3.2	430	3.1	38	1.0	4.6 [g]	3.8	57	0.83	13	2c
carbo [4]helicene	416	1.0	426	1.8	10	1.8	3.9 [g]	2.3	61	0.59	13	2d

Type	λ_{max}[b] (exp)	g_{abs}[c] (exp)	λ_{em}[b] (exp)	g_{lum}[c] (exp)	Stokes Shift[b] (exp)	g_{lum}/g_{abs} (exp)	g_{abs}[c] (calc)	g_{lum}[c] (calc)	Stokes Shift[b] (calc)	g_{lum}/g_{abs} (calc)	Reference	Molecule[d]
carbo [4]helicene	395	4.0	429	3.6	34	0.9	4.9 [g]	4.6	48	0.94	13	2e
carbo [4]helicene	400	1.6	435	0.2	35	0.12	–	0.5	–	–	13	2f
carbo [5]helicene	435	3.0	475	3.0	40	1.0	2.9 [g]	3	63	1.0	13	2p
carbo [6]helicene	409	10.8	430	3.4	21	1.9	1.0 [g]	4.1	35	4.1	13	2x
carbo [7]helicene	430	2.6	470	1.3	40	0.5	1.6	1.2	–	0.75	14	1
carbo [7]helicene	414	2.9	491	2.6	77	0.9	2.1	1.5	–	0.71	14	2

[a] Papers containing both experimental and TDDFT-calculated data were considered. Data for metallohelicenes, double helicenes and vibronic calculations were not included. – = not available. [b] In nm. [c] Multiplied by 10^3. [d] Molecule numbering or short name used in the original publication [e] Data in DCM. [d] Data in CAN. [f] Opposite sign; not included in the statistics. [g] Data courtesy of Gregory Pieters.
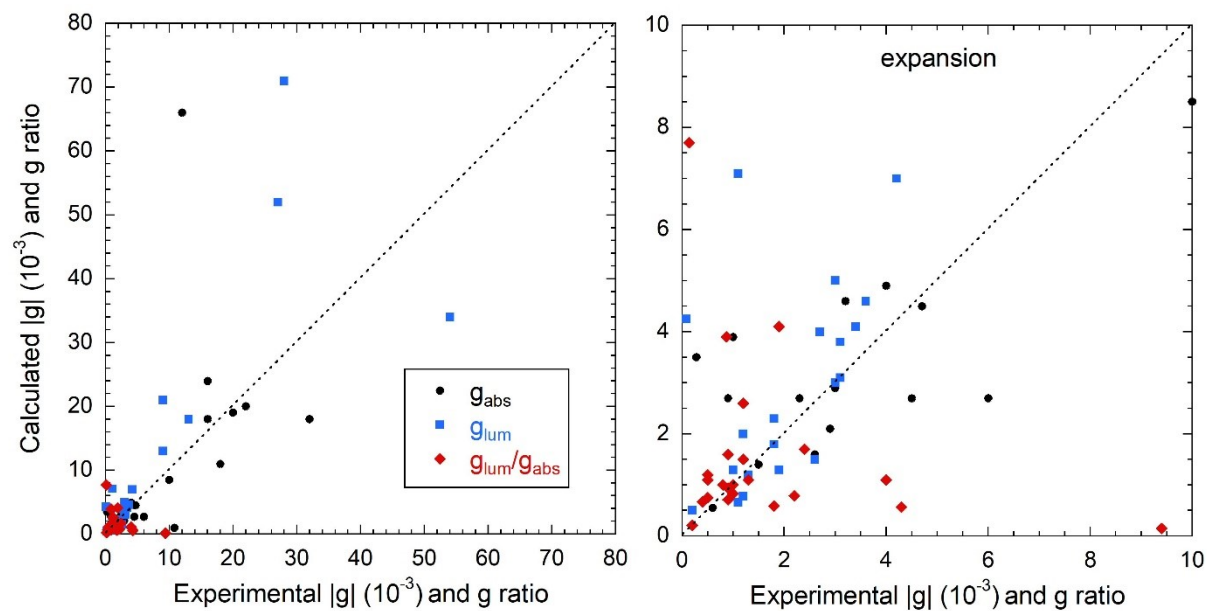
Figure S1. Comparison of GS (dark orange) and ES (green) geometries of *M*-**1a**, *M*-**2a** and *M*-**3** calculated at PBE0-1/3-D3BJ/6-311+G(d,p) level in the gas phase, seen along the C_2 axis. Hydrogen atoms removed for clarity.
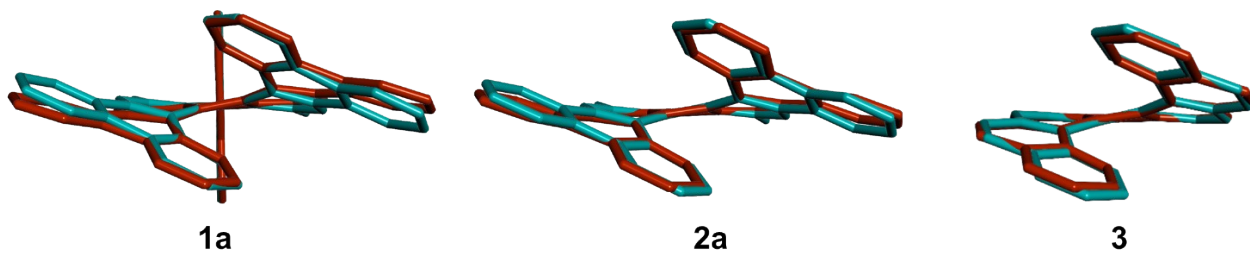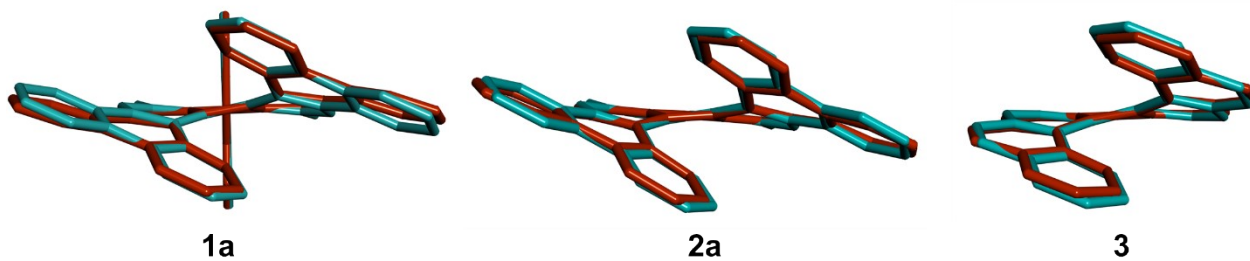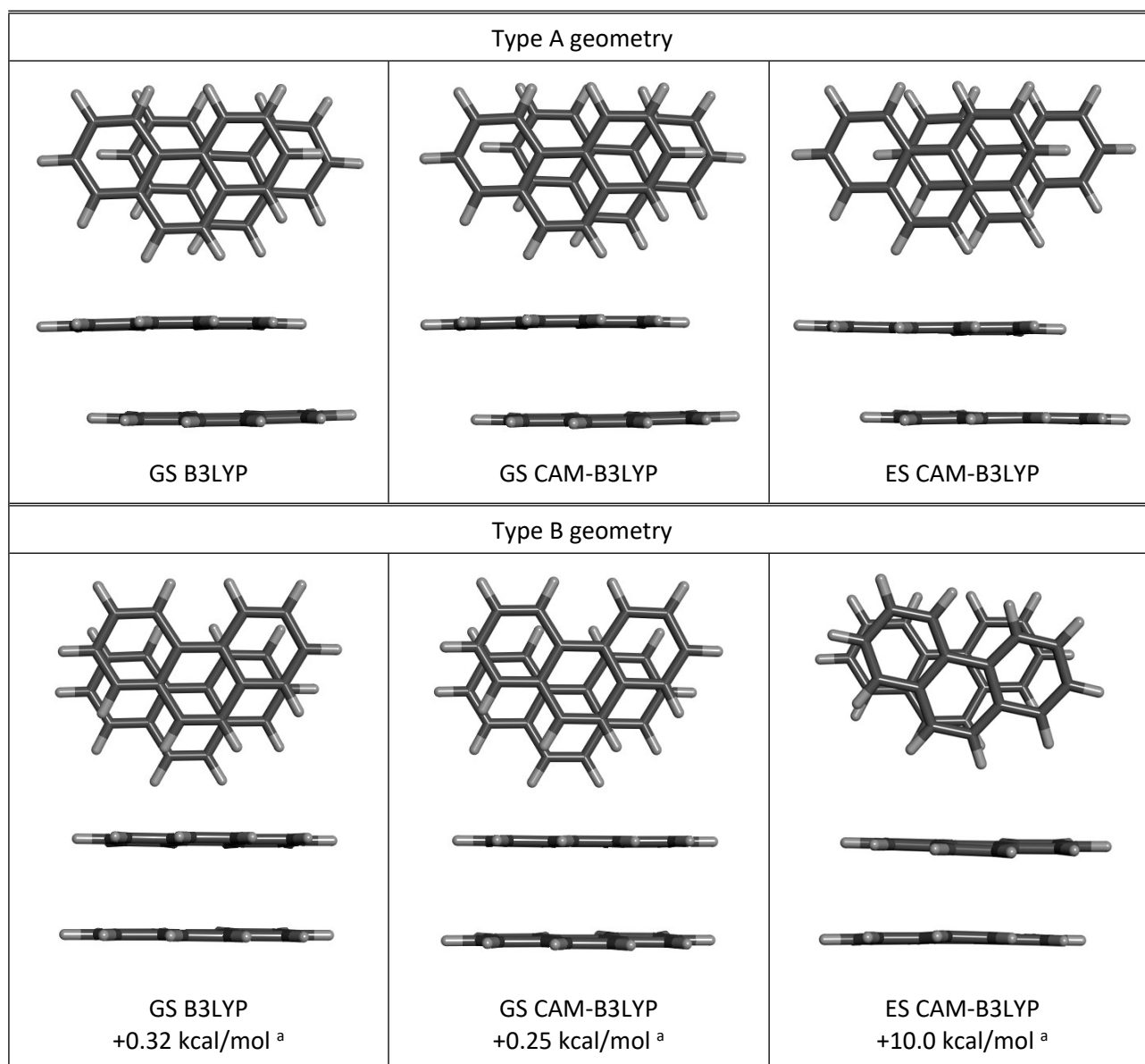

| **1a** | **2a** | **3** |

Figure S2. Comparison of GS (dark orange) and ES (green) geometries of *M*-**1a**, *M*-**2a** and *M*-**3** calculated at (CAM)-B3LYP-D3BJ/6-311+G(d,p) level in the gas phase, seen along the C_2 axis. Hydrogen atoms removed for clarity.


| **1a** | **2a** | **3** |

Figure S3. Selected geometries and energies for (TD)-DFT optimized ground-state (GS) and excited-state (ES) structures of phenanthrene stacked dimers **Phen$_2$**. All calculations run with D3BJ dispersion correction and 6-311+G(d,p) basis set. Top and side views are shown for each geometry.

Type A geometry		
GS B3LYP	GS CAM–B3LYP	ES CAM–B3LYP

Type B geometry		
GS B3LYP +0.32 kcal/mol [a]	GS CAM–B3LYP +0.25 kcal/mol [a]	ES CAM–B3LYP +10.0 kcal/mol [a]

[a] Relative internal energy with respect to Type A geometry optimized at the same level.

Figure S4. Geometries of (TD)-DFT optimized ground-state (GS) and excited-state (ES) structures of dimers (*M*,*M*)-**2a₂**. Calculations run with B3LYP (GS) and CAM-B3LYP (ES) functionals, D3BJ dispersion correction, 6-31+G(d) basis set and LR-PCM solvent model for CHCl₃. Top and side views are shown for each geometry. The two molecules are depicted with different colors for carbon atoms for clarity.

GS

ES
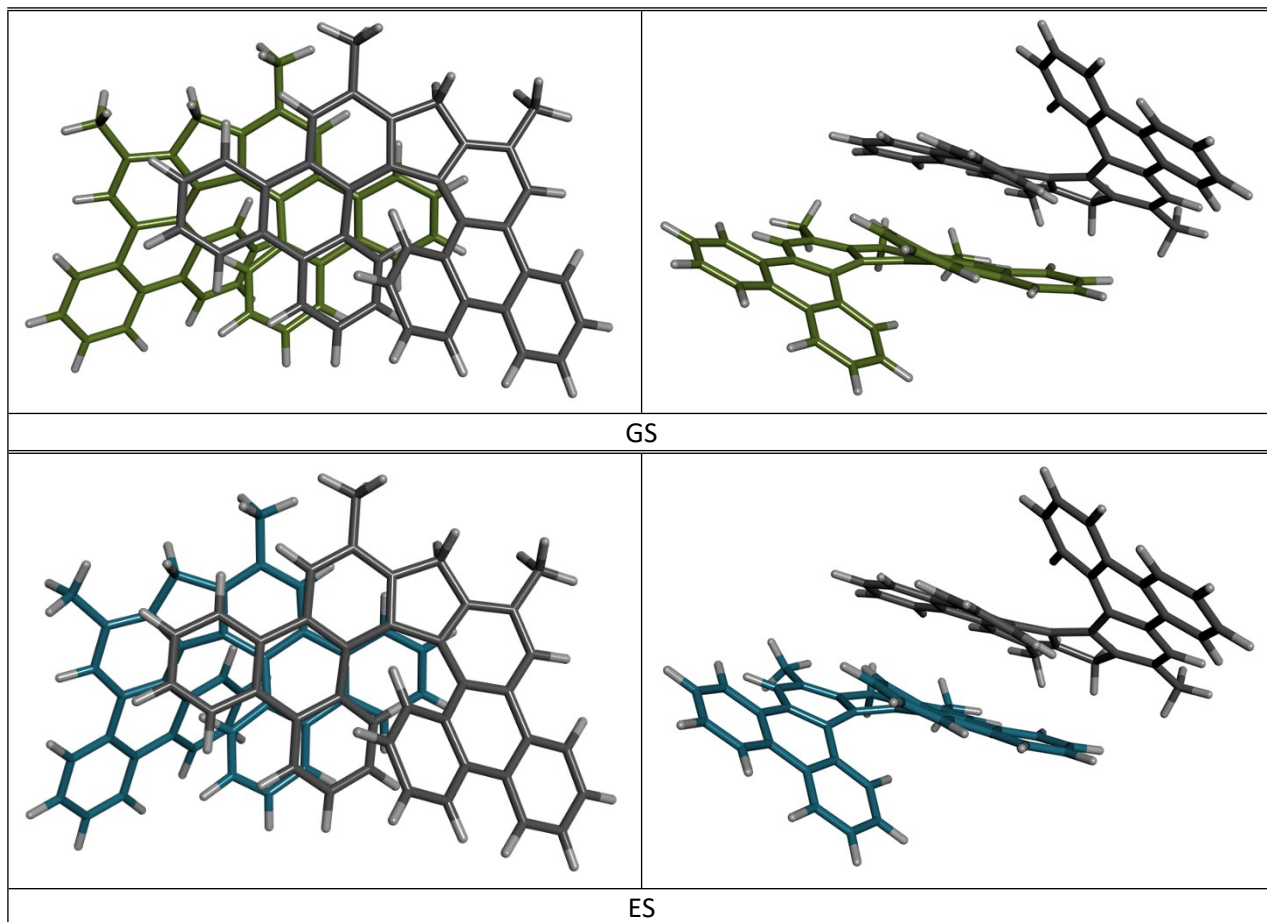
State-specific (SS) description of emission dissymmetry factors

The simulation of emission dissymmetry factors involves the optimization of the excited state geometry of the state of interest, possibly including solvation effects at state-specific (SS) level of theory. Indeed, as explained in the main text, limiting to just a Linear Response (LR) approach one only partially approximates the dispersion interactions between solute and solvent, whereas SS solvation approaches explicitly account for the change in the solvent polarization to adapt to the change in the system charge density upon the electronic transition. For a detailed discussion of how to describe the environment polarization response to electronic transitions, see refs. 15 and 16.

In principle both effects (i.e., SS polarization and dispersion) should be taken into account to properly describe solute-solvent interactions (as demonstrated in ref. 17). However, until now, excited-state energy gradients at TD-DFT level are only available for the SS VEM-PCM approach and the LR-PCM separately, and therefore we included the main polarization effects by the following steps:

i)   first, we optimize the GS structure in solvent using the IEF-PCM formalism (point 1 of Fig. S5);
ii)   then, we use the VEM approach in a *nonequilibrium regime* to simulate the absorption and ECD processes (step 2 of Fig. S5) on top of the GS optimized structure;
iii) finally, we optimize (step 3 of Fig. S5) the ES structures with the VEM energy gradients in an equilibrium regime, obtaining also the related properties necessary to compute g_{lum}, that is, the electric transition dipolar strengths and rotational forces (in the so-called velocity gauge).

These last quantities are indeed automatically calculated by the code using the converged transition densities of the self-consistent and state specific VEM algorithm on top of the optimized structure obtained as the last step of the VEM-UD optimization procedure (point 4 of Fig. S5). We finally recall that the emission energy requires a two-step calculation, in analogy with what has been already detailed in a white paper from Guido and Caprasecca[18] concerning the corrected Linear Response approach (note however that for cLR gradients are not implemented and only energies are corrected: VEM-UD is the only TDDFT-PCM state-specific approach for which gradients are defined).

We conclude pointing out that, the code for VEM-UD gradients is not already available in the public release of the G16 version of the Gaussian software, but all the implementation details of the VEM-UD gradients are reported in ref. 19.

Figure S5. Schematic illustration the steps necessary to compute emissive properties in a state specific approach.
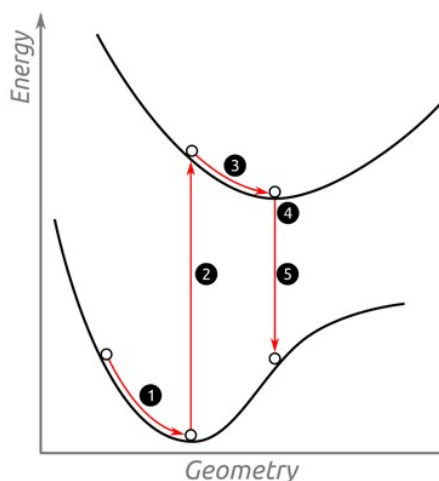
References for the Supporting Information

1. Y. Sawada, S. Furumi, A. Takai, M. Takeuchi, K. Noguchi and K. Tanaka, *J. Am. Chem. Soc.*, 2012, **134**, 4080-4083.
2. H. Oyama, M. Akiyama, K. Nakano, M. Naito, K. Nobusawa and K. Nozaki, *Org. Lett.*, 2016, **18**, 3654-3657.
3. F. P. A. Fabbiani, D. R. Allan, W. I. F. David, S. A. Moggach, S. Parsons and C. R. Pulham, *CrystEngComm*, 2004, **6**, 505-511.
4. S. Abbate, G. Longhi, F. Lebon, E. Castiglioni, S. Superchi, L. Pisani, F. Fontana, F. Torricelli, T. Caronna, C. Villani, R. Sabia, M. Tommasini, A. Lucotti, D. Mendola, A. Mele and D. A. Lightner, *J. Phys. Chem. C*, 2014, **118**, 1682-1695.
5. K. Dhbaibi, L. Favereau, M. Srebro-Hooper, C. Quinton, N. Vanthuyne, L. Arrico, T. Roisnel, B. Jamoussi, C. Poriel, C. Cabanetos, J. Autschbach and J. Crassous, *Chem. Sci.*, 2020, **11**, 567-576.
6. H. Kubo, T. Hirose, T. Nakashima, T. Kawai, J. Y. Hasegawa and K. Matsuda, *J. Phys. Chem. Lett.*, 2021, **12**, 686-695.
7. G. Longhi, E. Castiglioni, C. Villani, R. Sabia, S. Menichetti, C. Viglianisi, F. Devlin and S. Abbate, *J. Photochem. Photobiol. A: Chem.*, 2016, **331**, 138-145.
8. B. Mahato and A. N. Panda, *J. Phys. Chem. A*, 2022, **126**, 1412-1421.
9. Y. Nakakuki, T. Hirose and K. Matsuda, *Org. Lett.*, 2022, **24**, 648-652.
10. K. Usui, N. Narita, R. Eto, S. Suzuki, A. Yokoo, K. Yamamoto, K. Igawa, N. Iizuka, Y. Mimura, T. Umeno, S. Matsumoto, M. Hasegawa, K. Tomooka, Y. Imai and S. Karasawa, *Chemistry*, 2022, **28**, e202202922.
11. K. Dhbaibi, L. Abella, S. Meunier-Della-Gatta, T. Roisnel, N. Vanthuyne, B. Jamoussi, G. Pieters, B. Racine, E. Quesnel, J. Autschbach, J. Crassous and L. Favereau, *Chem. Sci.*, 2021, **12**, 5522-5533.
12. E. Yen-Pon, F. Buttard, L. Frederic, P. Thuery, F. Taran, G. Pieters, P. A. Champagne and D. Audisio, *JACS Au*, 2021, **1**, 807-818.
13. S. M. Guo, S. Huh, M. Coehlo, L. Shen, G. Pieters and O. Baudoin, *Nat. Chem.*, 2023, **15**, 872-880.
14. A. Swain and P. Ravat, *Org. Chem. Front.*, 2023, DOI: 10.1039/D3QO00386H.
15. C. A. Guido and S. Caprasecca, *Int. J. Quantum Chem.*, 2019, **119**, e25711.
16. C. A. Guido, A. Chrayteh, G. Scalmani, B. Mennucci and D. Jacquemin, *J. Chem. Theory Comput.*, 2021, **17**, 5155-5164.
17. C. A. Guido, M. Rosa, R. Cammi and S. Corni, *J. Chem. Phys.*, 2020, **152**.
18. https://molecolab.dcci.unipi.it/images/tools_dwld/PisaLR.pdf
19. C. A. Guido, G. Scalmani, B. Mennucci and D. Jacquemin, *J. Chem. Phys.*, 2017, **146**, 204106.